This is a preprint, the final version is subject to change, of the American Mineralogist (MSA)
Cite as Authors (Year) Title. American Mineralogist, in press.
(DOI will not work until issue is live.) DOI: http://dx.doi.org/10.2138/am-2017-5860

Revision 2

High-resolution geochemistry of volcanic ash highlights complex magma dynamics during the Eyjafjallajökull 2010 eruption

Kathrin Laeger[1]*, Maurizio Petrelli[1], Daniele Andronico[2], Valeria Misiti[3], Piergiorgio Scarlato[3], Corrado Cimarelli[4], Jacopo Taddeucci[3], Elisabetta del Bello[3], and Diego Perugini[1]

[1] Department of Physics and Geology, University of Perugia, Piazza dell'Università 1, 06123 Perugia, Italy

[2] Istituto Nazionale di Geofisica e Vulcanologia, Sezione di Catania, Osservatorio Etneo, Piazza Roma 2, 95125 Catania, Italy

[3] Istituto Nazionale di Geofisica e Vulcanologia, Via di Vigna Murata 605, 00143 Rome, Italy

[4] Department of Earth and Environmental Sciences, University of Munich, Theresienstraße 41, 80333 Munich, Germany

* *Corresponding author:*

E-mail: kathrin.laeger@studenti.unipg.it

Tel.: +390755852652

Fax: +390755852603

Always consult and cite the final, published document. See http:/www.minsocam.org or GeoscienceWorld

This is a preprint, the final version is subject to change, of the American Mineralogist (MSA)
Cite as Authors (Year) Title. American Mineralogist, in press.
(DOI will not work until issue is live.) DOI: http://dx.doi.org/10.2138/am-2017-5860

Abstract

The April-May 2010 eruption of Eyjafjallajökull (Iceland) volcano was characterized by a large compositional variability of erupted products. In order to contribute to the understanding of the plumbing system dynamics of this volcano, we present new EMPA and LA-ICP-MS data on groundmass glasses of ash particles and minerals erupted between April 15th and 22nd. The occurrence of disequilibrium textures in minerals, such as resorption and inverse zoning, indicate that open system processes were involved in determining the observed compositional variability. The variation of major and trace element data of glasses corroborates this hypothesis indicating that mixing between magma batches with different compositions interacted throughout the whole duration of the eruption. In particular, the arrival of new basaltic magma into the plumbing system of the volcano destabilized and remobilized magma batches of trachyandesite and rhyolite compositions that, according to geophysical data, might have intruded as sills over the past twenty years beneath the Eyjafjallajökull edifice. Two mixing processes are envisaged to explain the time variation of the compositions recorded by the erupted tephra. The first occurred between basaltic and trachyandesitic end-members. The second occurred between trachyandesite and rhyolites. Least squares modeling of major elements supports this hypothesis. Furthermore, investigation of compositional histograms of trace elements allows us to estimate the initial proportions of melts that interacted to generate the compositional variability triggered by mixing of trachyandesites and rhyolites.

Keywords: Eyjafjallajökull, volcanic ash, magma mixing, plumbing system dynamics.

Always consult and cite the final, published document. See http:/www.minsocam.org or GeoscienceWorld

Introduction

On March 20th 2010, a mainly effusive fissure eruption at the flank of Eyjafjallajökull (EFJ) volcano began, changing to an explosive phase from the summit on April 14th, lasting until the end of May (Sigmundsson et al. 2010). During this time frame, a large amount of ash was injected into the atmosphere and transported towards Europe and the North Atlantic area. This caused a disruption of the European air traffic, forcing millions of passengers to stay grounded, and producing a huge economic loss of several hundred million US dollars per day, as industrial production had to stop in the affected parts of Europe (Miller 2011; O'Regan 2011; Guðmundsson et al. 2012).

Several works suggest that the eruption was initiated by arrival of new basaltic magma into the shallow plumbing system of the volcano initiating mingling and mixing by transporting mass, heat and volatiles (e.g. Sigmundsson et al. 2010; Sigmarsson et al. 2011, 2015; Borisova et al. 2012; Viccaro et al. 2016). Initially, a Fe-Ti-basalt erupted effusively. The successive explosive activity mainly emitted trachyandesite tephra, intermingled with more evolved basalts and trachyandesite to trachydacite compositions. Borisova et al. (2012) pointed out that those more evolved basalts occurring together with the trachyandesite tephra were produced by mixing of the Fe-Ti-basalt with a trachydacite magma. Trachyandesite melts were considered by Borisova et al. (2012) as the product of further mixing between the more evolved basalt and trachydacites. Support to this hypothesis was provided by the occurrence of olivine, clinopyroxene and plagioclase phenocrysts displaying bimodal compositions (Sigmarsson et al. 2011; Borisova et al. 2012; Keiding and Sigmarsson 2012). However, Sigmarsson et al. (2011) indicated that trachyandesites possibly represented the hybrid composition resulting from

Always consult and cite the final, published document. See http:/www.minsocam.org or GeoscienceWorld

mixing between an older silicic component and Fe-Ti-basalts. Despite the variation of end-members envisaged by the different authors, it is noteworthy that both studies focus the origin of trachydacite melts in the reheating and remobilization of a rhyolitic magma body that possibly remained in the plumbing system of the volcano since AD 1821-23 eruption. However, although magma mixing is undoubtedly involved in generating the large compositional variability shown by EFJ 2010 eruptive products, some issues related to the precise identification of potential end-members that took part to the magma mixing processes still remains unclear. This is essential to define the most complete picture for EFJ 2010 plumbing system dynamics and eruption.

In this work, we report a large number of new major and trace element data on minerals and glasses from ash particles and lava clasts erupted during the explosive phases of EFJ 2010 eruption, with the aim to shed new light on the complex processes that characterized this eruption. Geochemical modeling is coupled with petrographic observations and mineral chemistry data to refine existing petrological models for EFJ 2010 eruption and better constrain plumbing system dynamics. We finally propose an attempt to refine the model for the pre- and syn-eruptive plumbing system of EFJ 2010 combining geophysical evidence, petrological data, and geochemical modeling.

Geologic setting of Eyjafjallajökull volcano and the 2010 eruption

Eyjafjallajökull rises 1666 m a.s.l. on the south coast of Iceland. It is located around 30 km to the southeast of the town Hvolsvöllur and 15 km to the west of the Mýrdalsjökull glacier and Katla volcano (Fig. 1). EFJ volcano belongs to the Eastern Volcanic Zone (EVZ), together with Katla, the Vestmanneyar archipelago and Surtsey

Always consult and cite the final, published document. See http:/www.minsocam.org or GeoscienceWorld

(Hjaltadóttir et al. 2009; Sturkell et al. 2010). Known eruptive events have occurred over the last 1500 years, these include radial fissure eruptions such as AD 920, and small summit eruptions in AD 1612/13 and in AD 1821–23 (Loughlin 1995; Larsen et al. 1999; Sigmundsson et al. 2010). The eruption between 1821 and 1823 produced a tephra volume of 0.004 km^3 of rhyolitic composition (Larsen et al. 1999). In general, lava flows from fissure eruptions were mainly basaltic and basaltic-andesitic in composition. However, summit eruptions have emitted both effusive and explosive products (lavas and tephra) with SiO_2 contents ≥55 wt% (Sigmundsson et al. 2010).

Ground deformation and seismic activity occurred during the 1990s at Eyjafjallajökull indicating sill intrusion between 3.5-6.5 km and 19-25 km depth from the top crater (Dahm and Brandsdóttir 1997; Sturkell et al. 2003, 2006, 2010; Pedersen and Sigmundsson 2004, 2006; Hooper 2008; Hooper et al. 2009; Hjaltadóttir et al. 2009, 2015; Guðmundsson et al. 2010). EFJ 2010 eruption can be divided into different phases based on timing, eruptive style and composition of erupted materials. Phase I started on March 20th as a fissure flank eruption that lasted until April 12th. Two scoria cones and a lava flow consisting of ca. 0.02 km^3 of high Fe-Ti-basalt were generated through lava fountains and minor tephra falls (Sigmarsson et al. 2011; Edwards et al. 2012; Cioni et al. 2014). After a two-day hiatus and a seismic swarm from ca. 5 km depth (Karlsdóttir 2012), a powerful explosive summit eruption occurred in the morning of April 14th and lasted with irregular activity until May 22nd. This explosive activity, named as Phase II, can be divided into two main phases. At its beginning (from April 14th-18th) Phase IIa was mainly phreatomagmatic, and was accompanied by a widespread dispersal of fine ash into the atmosphere, up to 9 km a.s.l. On April 19th the plume height decreased to 3-4

Always consult and cite the final, published document. See http:/www.minsocam.org or GeoscienceWorld

km and the eruption became magmatic with both explosive and effusive activity. On May 3rd, seismicity was detected at 18-23 km depth, followed by shallower events between 4 and 20 km until May 4th; this was interpreted as the injection of new basaltic magma (Guðmundsson et al. 2012; Tarasewicz et al. 2012b, Hjaltadóttir et al. 2015). Phase IIb started around May 5th, with explosive activity (plume height ca. 9 km a.s.l.); at this stage lava flows stopped completely (Guðmundsson et al. 2010; Sigmarsson et al. 2011; Sigmundsson et al. 2012). On May 10th-11th and May 15th, further deep seismic swarms at 20-24 km depth were recorded, whilst shallow micro-earthquakes proceeded throughout May (Tarasewicz et al. 2012a, b). From May 18th to 22nd, the plume declined and the activity ended. The total erupted mass (lava plus tephra) was estimated at $4.7\pm1.2\times10^{11}$ kg, corresponding to a Dense Rock Equivalent (DRE) of ca. 0.18 ± 0.05 km^3 (Guðmundsson et al. 2012).

Analytical methods

Sampling and sample preparation

The majority of the samples were erupted between May 18th and 22nd, 2010. Sample collection was carried out by the Istituto Nazionale di Geofisica e Vulcanologia Rome (INGV, Italy; E1-E41). Further ash samples of the explosive activity have been provided by C. Horwell (Horwell et al. 2013; samples EYJ_10_01-13, 15.04.-07.05.2010), A. Vogel (Norwegian Institute of Air Research, Norway; V-EJ 01-03, 16.-18.04.2010) and H. Tuffen (Lancaster University, UK; T-EJ 01, 22.04.2010). All sample locations are shown in Figure 1. Coordinates of sample locations and complete geochemical characterization of samples are provided in the Supplementary Material

Always consult and cite the final, published document. See http:/www.minsocam.org or GeoscienceWorld

Table i.

Electron microprobe analysis (EMPA)

Major element concentrations of glasses were determined analysing one spot per ash particle with a JEOL JXA 8200 at the INGV facilities in Rome. The EMPA is equipped with five wavelength-dispersive spectrometers and 12 crystals. The electron beam had a current of 10 nA, an accelerating voltage of 15 keV and a defocused beam diameter of 10 μm. The acquisition times for the glasses were 10 s for the peak and 5 s for the background. Synthetic and natural standards were used for calibration. In detail: anorthoclase NMNH 133868 (Si, standard deviation σ = 0.01; Al, σ = 0.01; Jarosewich et al. 1980), anorthite NMNH 137041 (Ca, σ = 0.03; Jarosewich et al. 1980), augite NMNH 122142 (Mg, σ = 0.04; Fe, σ = 0.02 Jarosewich et al. 1980), rutile MAC T-1154 (Ti, σ = 0.07; Micro-Analysis Consultants Ltd.), MAC orthoclase (K, σ = 0.01; Micro-Analysis Consultants Ltd.), MAC apatite (P, σ = 0.10; Micro-Analysis Consultants Ltd.) and MAC rhodonite (Mn, σ = 0.30; Micro-Analysis Consultants Ltd.). Sodium and potassium were analysed first to reduce possible volatilization effects. ZAF correction routines (Armstrong and Buseck 1975) were used to obtain element concentrations.

Laser ablation inductively coupled plasma quadrupole mass spectrometry (LA-ICP-QMS)

Trace element concentrations of matrix glasses were determined by analyzing the exact spots measured with the EMPA at the Department of Physics and Geology (University of Perugia, Italy) using a Teledyne/Photon Machine G2 laser ablation system

Always consult and cite the final, published document. See http:/www.minsocam.org or GeoscienceWorld

equipped with a Two-Volume ANU (Australian National University) ELEX 2 cell and coupled with a Thermo Fisher Scientific ICP-QMS. Ablation was performed under a He atmosphere, using a laser beam with a diameter fixed at 8 μm and a repetition rate of 8 Hz. The background acquisition, ablation, and washout time was 20 s each for a total duration of 60 s per analytical determination. The NIST-SRM-610 glass reference material (Pearce et al. 1997) was utilized as external calibrator and ^{29}Si was employed as an internal standard. The USGS BCR2G (Wilson 1997) was used as quality control. The data reduction was completed using the Iolite 3 software (Paton et al. 2011), following the protocol reported in Longerich et al. (1996). Further details on the technique are given in Petrelli et al. (2016a, 2016b).

Results

Petrography and mineral chemistry

The studied tephra fragments mainly consist of ash particles (0.2-2.0 mm) and pumice clasts (20-50 mm). Pumices are highly vesiculated, whereas ash fragments can be both, highly or sparsely porous (Fig. 2a). A glassy and sparsely-crystalline groundmass alternates with fully crystalline parts. The latter also occur as single ash particles. The main mineral phases occurring in the ash fragments are represented by plagioclase (Pl, 20 vol%, ≤4 mm), clinopyroxene (Cpx, 5-10 vol%, ≤0.5 mm) and olivine (Ol, 5 vol%, ≤2 mm). Fe-Ti-oxides (Mgt, ≤0.1 mm) and apatite (Ap, ≤0.2 mm) occur as accessory phases. Mineral compositions were determined by EMPA; the complete mineral chemistry dataset is reported in the Supplementary Material (Tables iii-vii). Pl mostly occurs as elongated euhedral and subhedral crystals; this mineral is also present as fragmented

Always consult and cite the final, published document. See http:/www.minsocam.org or GeoscienceWorld

grains and glomerocrysts together with Cpx, Ol and Mgt. Most of Pl displays compositional zoning with inner zones having anorthite contents from An_{81} to An_{53}; outer zones generally display lower anorthite contents in the range An_{46-13} (Fig. 2c). Lower anorthite content Pl (An_{36-10}) also occurs mainly with disequilibrium sieve textures in which incipient melting of the plagioclase is also observed (Fig. 2d). Cpx is euhedral to subhedral and characterized by normal (Mg# from 44 to 67) and reverse zoning ($Mg\#_{Core}$=51-60, $Mg\#_{Rim}$=56-71). Reverse zoning in Cpx is commonly accompanied by strongly corroded cores followed by euhedral overgrowth (Fig. 2f). Ol occurs as homogeneous euhedral and subhedral normal zoned crystals, commonly containing chromium spinel inclusions (Fig. 2c, e). Ol Mg# contents vary in the range of Fo_{83-74} for cores and Fo_{67-48} for rims. Fe-Ti-oxides are euhedral to anhedral and comprise mainly Ti-magnetite (48-93 mol% Usp), with few chromium spinel and scarce ilmenite (87 mol%).

In general, from mineral chemistry data it appears that a large compositional complexity is associated with mineral phases occurring in the ash samples with normal, reverse and resorptions textures of the same mineral phases occurring side by side at short length scale, even in the same ash sample.

Chemical variability of Eyjafjallajökull 2010 products

A total of 801 and 186 acquisitions were performed on glasses for major and trace elements, respectively. The complete geochemical dataset is given in Table ii in the Supplementary Material.

Figure 3 reports total alkali versus silica diagrams (TAS; Le Bas et al. 1986) for the erupted samples divided into phases of the eruptive activity. The plots have been

Always consult and cite the final, published document. See http:/www.minsocam.org or GeoscienceWorld

constructed using both available literature data (Sigmundsson et al. 2010; Sigmarsson et al. 2011; Keiding and Sigmarsson 2012; Borisova et al. 2012; Cioni et al. 2014) and new data of groundmass glasses (GL) collected during the present work. Glass compositions of the EFJ 1821-1823 eruption (named RH1821; Larsen et al. 1999; Sigmarsson et al. 2011) are also reported in Figure 3a.

Phase I (20.03-12.04.2010) is characterized by an almost homogeneous basaltic composition with SiO_2 content in the range of 46-48 wt%. Hereafter, we define this composition as WR BAS I and GL BAS I by referring to the whole rock (WR) and groundmass glass (GL) composition, respectively (Fig. 3a). Phase II (14.04-22.05.2010) is characterized by a larger compositional variability of the samples. In particular, a more evolved basalt (named BAS II; 50-52 wt% SiO_2) appears during Phase IIa and IIb; its abundance decreases towards the end of eruption, as shown by the decreasing number of samples having this composition towards Phase IIb. In Phase IIa glasses with silica contents from 57.6 to 70.1 wt% SiO_2 also appear (Fig. 3a). These samples show compositional gaps between approximately 61 and 68 wt% SiO_2. In Phase IIb the same compositional span observed in Phase IIa is continuous and the gaps disappear (Fig. 3b). We name this compositional range 'TA-RH' (trachyandesite-rhyolite). BAS II and TA-RH are separated by a compositional gap of ca. 4 wt% SiO_2 (Fig. 3). Some representative variation diagrams of major and trace elements versus SiO_2 for Phase II are reported in Figure 4 and 5. In general, TiO_2, FeO, MgO, CaO and P_2O_5 correlate negatively with SiO_2; Al_2O_3 remains almost constant, with some scattering, whereas Na_2O and K_2O correlate positively with SiO_2 (Fig. 4). Figures 5a-c show a positive correlation between highly incompatible elements, such as Th, Zr and U, and SiO_2. Ba is also increasing as

Always consult and cite the final, published document. See http:/www.minsocam.org or GeoscienceWorld

SiO_2 increases. Conversely Sr and V abundances decrease as the silica content increases (Fig. 5d-f). A spider diagram normalized to ocean island basalts (Sun and McDonough 1989) is displayed in Figure 6 and summarizes the general features of trace elements of studied samples. It shows a slight enrichment of trace elements in TA-RH glasses, with the exception of Sr, P and Ti, which display negative anomalies. BAS I and BAS II have a very similar signature and show lower abundances of trace elements compared to TA-RH.

Discussion

Geochemical processes leading to the compositional variability of Eyjafjallajökull 2010 products

As introduced above, the refilling of a shallow plumbing system by more mafic magma coming from deeper levels is considered to be the process that likely triggered the EFJ 2010 eruption (Sigmundsson et al. 2010; Sigmarsson et al. 2011, Borisova et al. 2012). This idea is also generally supported by our data and, in particular: i) phenocryst populations display a great compositional variability and disequilibrium textures (e.g. normal, reverse, and oscillatory zoning, resorptions patterns, etc.; Fig. 2) that point towards the hypothesis that open system processes, such as magma mixing (e.g. Hibbard, 1981) must have played a role in their formation; ii) ash compositions show a huge compositional variability ranging from basaltic to rhyolitic (Fig. 2a, b and Fig. 3) at very short length scales (of the order of the same ash sample), indicating that different melts coexisted immediately before and/or during the eruption.

Always consult and cite the final, published document. See http:/www.minsocam.org or GeoscienceWorld

These features clearly suggest that magma interaction might have been crucial in determining the geochemical variability and the petrographic characteristics observed in the erupted rocks. However, other features, such as the decreasing trend of V (Fig. 5f) and the Sr, P, and Ti depletions observed in the spider diagram (Fig. 6) may indicate that additional differentiation processes, such as fractional crystallization, may have contributed to determine the geochemical variability observed in the erupted products. In the attempt to decipher which petrogenetic process played a major role, we performed a complete set of geochemical models considering both fractional crystallization and magma mixing as possible end-member processes that might have been involved in the generation of the compositional variability of EFJ 2010 eruption.

With regards to fractional crystallization, we modeled liquid lines of descent (LLD) starting from different parental compositions. The modeling was performed using the software MELTS at different pressures (0.5-8.0 kbars), water contents (0.0-2.5 wt%) and oxygen buffers (i.e. NNO and QMF). Some representative plots illustrating the LLD arising from the modeling for MgO and CaO are reported in Figure 7. Complete information, including models for all major elements at the different conditions, are given in the Supplementary Material. Models were generated using as potential parental melts average compositions of WR BAS I, GL BAS I and GL BAS II (Fig. 7). Further modeling was also performed considering TA as a potential parental magma from which the whole TA-RH geochemical variability might have been generated. The plots shown in Figure 7 (as well as the complete set of models and plots reported in the Supplementary Material 'xi') clearly indicate that fractional crystallization cannot be considered as a petrogenetic process that played a major role in determining the observed

Always consult and cite the final, published document. See http:/www.minsocam.org or GeoscienceWorld

geochemical variability. In fact, while for some elements a given fractional crystallization model appears to work, it is unsuccessful for other elements. On the basis of these results, it is therefore very likely that fractional crystallization played a very minor role, if any, in determining the geochemical variability of ash samples during the Eyjafjallajökull eruption.

As shown above, both petrographic and geochemical features of studied rocks indicate that magma mixing is likely to have been involved in determining the observed compositional variability. Investigation of inter-elemental variation diagrams (Fig. 4 and 5) provides some constraints upon the possible end-members that may have been involved into the mixing process. These diagrams indicate that it is improbable that WR BAS I and RH were the end-members that mixed to generate the observed compositional variability. In fact, as a first approximation, mixing processes should generate linear variations in binary inter-elemental plots. Conversely, our inter-elemental diagrams (Fig. 4 and 5) clearly show non-linear patterns for some elements such as MgO, P_2O_5 or V, arguing against the hypothesis that BAS I and RH were the two initial end-members. The same reasoning is valid if we consider GL BAS I as basic end-member. In fact, this mixing process would not explain elements such as P_2O_5 and V variations. A further possibility is that multiple mixing processes occurred between different end-member couples throughout the instability of the magmatic systems that culminated in the eruption. In particular, it could be envisaged that WR BAS I or GL BAS I interacted with TA to generate BAS II. However, WR BAS I is not likely to represent a consistent end-member because, for the same reasoning made above, it would not explain the non-linear patterns shown by elements such as TiO_2, MgO and P_2O_5 (Fig. 4). On the contrary, GL

Always consult and cite the final, published document. See http:/www.minsocam.org or GeoscienceWorld

BAS I appears to have all the requirement to make a good candidate for the basic end-member. In fact, its interaction with TA would be able to produce intermediate compositions such as BAS II lying on a mixing line between GL BAS I and TA. Noteworthy is the fact that a compositional gap of ca. 4 wt% SiO_2 exists between ~52-56 wt% SiO_2. This evidence can be explained by an incomplete mixing process, possibly due to short mixing times, between the two end-members. Support for this hypothesis derives from experimental data on magma mixing (e.g. Morgavi et al. 2013a, b; Perugini et al. 2013), where compositional gaps are commonly observed for short-time mixing experiment.

The other magma mixing process that can be envisaged is between TA and RH. From the observation of both major and trace elements variation diagrams (Fig. 4 and 5) it appears, however, that while for some major elements a binary mixing process (i.e. a linear trend between TA and RH) appears plausible, for other major elements more complex (generally scattered) trends appear to undermine this hypothesis. The same applies for trace elements that display variable degrees of scattering of data points on binary diagrams (Fig. 8). Recently published data on magma mixing experiments performed using natural compositions (e.g. Morgavi et al. 2013a, b; Perugini et al. 2013) highlighted a general deviation from the classic two end-member mixing process (i.e. linear trend in inter-elemental plots) towards scattered plots, due to different mobility of both major and trace elements. Deviation from linear trends towards scattered patterns becomes progressively more evident as the mixing process progresses in time. In particular, linear trends are observed only when two chemical elements have the same mobility in the magmatic mass (e.g. Perugini et al. 2008). Binary plots in Figure 4

Always consult and cite the final, published document. See http:/www.minsocam.org or GeoscienceWorld

illustrate that certain major elements (such as MgO vs. SiO_2 and CaO vs. SiO_2) display linear patterns. When element couples such as K_2O and SiO_2 are considered, the scattering appears evident. All major elements are generally regarded to have approximately the same mobility due their similar diffusivities in silicate melts (e.g. Baker 1990), with the exception of K_2O and Na_2O that are regarded as having larger diffusivities (Baker 1990). This general variability of chemical element mobility can explain the behavior of major elements during mixing as observed for Eyjafjallajökull data. As for trace elements, they are typically regarded as having larger diffusivities (and hence mobility) compared to major elements. The scattered behavior shown in Figure 5 between the different trace elements and SiO_2 supports this hypothesis. Figure 8 shows inter-elemental binary plots for some representative couples of trace elements. These plots show that, while for some couples of elements linear relationships arise (compatible with a two end-member mixing process), other couples display variable degrees of scattering. As in the case of major elements these features can be attributed to the different mobility of trace elements during mixing; elements with similar mobility tend to display linear patterns, whereas elements with different mobility show progressively larger degrees of scattering (e.g. Perugini et al. 2013). It is worth noting that the variable degree of scattering observed in inter-elemental plots is observed only for the second envisaged mixing process (between TA and RH). With respect to this, it must be noted that the emergence of scattered patterns in inter-elemental diagrams tends to be progressively mode evident as the mixing process progresses in time (e.g. Perugini et al. 2008, 2013). As reported above, the mixing processes between GL BAS I and TA protracted for shorter time (as evidenced by the occurrence of the compositional gap)

Always consult and cite the final, published document. See http:/www.minsocam.org or GeoscienceWorld

relative to the mixing between TA and RH (i.e. continuous variation between the two end-members). This might explain the differences in the behavior of the different couples of chemical elements in the two mixing processes.

Along with the previous discussion, further observations favoring the magma mixing hypothesis are the presence of disequilibrium textures in minerals (e.g. resorptions and reverse zoning) and the occurrence of extreme compositional variability (from basalt to rhyolite) in the same ash sample. As shown by several works (Perugini et al. 2003, Slaby et al. 2011, Morgavi et al. 2013a), this strong compositional variability at very short length scale (of the order of hundreds of microns, i.e. the size of ash grains) is a typical feature arising from the development of chaotic dynamics during magma mixing processes. In particular, the development of fractal compositional patterns down to a few microns is the natural consequence of the scale-invariance associated with chaotic mixing processes. Fragmentation of magma volumes with such an extreme compositional variability during a volcanic eruption (as in the case of Eyjafjallajökull) would allow for the observation of a strong compositional variability even in the same ash sample, as indeed recorded for the EFJ 2010 eruption.

The above observations, therefore, allow us to hypothesize that two magma mixing processes might explain the observed chemical variability. In order to test these hypotheses in quantitative terms, mass balance calculations for major elements (Chayes 1968; Bryan et al. 1969; Störmer and Nicholls 1978), implemented within the software Petrograph (Petrelli et al. 2005) (Table 1) were performed. In particular, magma mixing mass balance calculations were performed considered the above-defined end-member couples, i.e. GL BAS I and TA (first mixing process) and TA and RH (second mixing

Always consult and cite the final, published document. See http:/www.minsocam.org or GeoscienceWorld

process). For the first mixing process we used the average compositions of GL BAS I (SiO_2 between 47.0-47.5 wt%) as mafic end-member the average composition of least evolved TA samples (SiO_2 between 57.0-57.9 wt%) for the felsic end-member. As for the second mixing process we used the same average values of TA considered above for the mafic end member and an average of most evolved RH compositions (SiO_2 between 67.8-70.0 wt%) for the felsic end-member. Results are presented in Table 1 and show that the sum of residuals from the least-square modeling are very low for both mixing processes, indicating the feasibility of these processes to explain the observed geochemical variability.

Estimation of initial proportions of mixed magmas

Perugini et al. (2004, 2008, 2013) suggested that the compositional variability generated during mixing could be utilized to estimate the initial proportions of end-member melts. With regards to this hypothesis, it should be noted that the ability of chemical elements to spread in magmatic systems (and, hence, to generate compositional variability) due to mixing can depend upon the combined effects of several processes such as (Perugini et al. 2015): 1) partitioning of chemical elements into structurally different melts (Watson 1976), 2) the dependence of diffusivities on multicomponent composition (Zhang 2008), 3) the influence of advection on apparent diffusive fluxes (Perugini et al. 2006) 4) the potential development of "uphill" diffusion patterns (Watson and Jurewicz 1984). Therefore, the compositional variability in mixing systems is the expression of the cumulative effects of these processes that ultimately define the element

Always consult and cite the final, published document. See http:/www.minsocam.org or GeoscienceWorld

"mobility". In the following we refer to chemical element mobility considering the definition provided above.

The approach of Perugini et al. (2004, 2008, 2013) relies upon the fact that, at the beginning of magma mixing, all chemical elements show a bimodal distribution with two modal values corresponding to the two end-member compositions (Perugini et al. 2004, 2008). As the mixing process proceeds in time, the frequency of end-member compositions gradually decreases, favoring the appearance of a progressively larger population of samples with the hybrid composition. In this case, the compositional histogram becomes a Gaussian distribution whose maximum corresponds to the hybrid concentration for a given chemical element (Perugini et al. 2004, 2008). The rate of production of hybrid magmas is proportional to the mobility of chemical elements in the mixing system. Therefore, fast diffusion species (e.g. Na) will homogenize faster than slow-diffusing elements (e.g. Si; Perugini et al. 2008). Consequently, mixing systems are generally characterized by a bimodal distribution of slow-diffusion elements and Gaussian bell-shaped distributions for fast-diffusing chemical elements (Perugini et al. 2008).

Although, in principle, this method can be potentially applied to any mixing process, it requires that mixing was prolonged for a sufficient length of time in order to generate a continuous range of compositions between the two end-members. The reason for this is that the larger the number of data points (samples) with intermediate compositions, the better the statistical evaluation of the hybrid composition. According to the discussion made above, the first mixing process that occurred between GL BAS I and TA shows a compositional gap indicating that the mixing process was not prolonged. In

Always consult and cite the final, published document. See http:/www.minsocam.org or GeoscienceWorld

contrast, the second mixing process generated a much larger compositional variability covering all intermediate compositions between the two end-members (TA and RH). As a consequence, the approach discussed above for the determination of end-member proportions can only be applied to the second mixing process.

Frequency histograms for representative elements of the EFJ 2010 samples in the compositional range TA-RH are displayed in Figure 9. The plots show that according to the above discussion, slow-diffusing species (e.g. SiO_2, TiO_2, FeO, Nb) are characterized by a bi-modal distribution (Fig. 9a-c, e). In contrast, fast diffusing elements (e.g. Na_2O and several trace elements) display bell-shaped Gaussian-like distributions (Fig. 9d, f-h). In order to estimate the proportion of the end-members involved in the magma mixing process, we first estimated the composition of the end-members by taking the two extreme compositional values for the slow-diffusing elements (Perugini et al. 2008). Then, we calculated the hybrid composition only for those elements showing a bell-shaped Gaussian profile utilizing the modal value of the distribution. Knowing the end-members and hybrid compositions, the initial proportion of felsic component (X) of the two interacting magmas can be estimated using the following relationship:

$$X = \frac{C_H - C_M}{C_F - C_M} \qquad (1)$$

where C_H, C_M, C_F are the concentrations of the hybrid, least evolved and most evolved melt, respectively (Perugini et al. 2004, 2008). Results are reported in Table 2 and indicate that the fraction of felsic magma participating to the mixing processes was ca. 0.41±0.06. This uncertainty is due to the small fluctuations in the estimate of C_H using the different chemical elements. As a consequence, the fraction of the more mafic end-member (i.e. TA) must have been of the order of 0.59.

Always consult and cite the final, published document. See http:/www.minsocam.org or GeoscienceWorld

Implications

The above presented results and discussions can be used to refine and better constrain the EFJ 2010 pre- and syn-eruptive plumbing system. Figure 10 is an illustration from Tarasewicz et al. (2012b) modified in light of the results reported in our work. During December 2009 and February 2010 seismic activity was recorded at shallow depth (ca. 4.5-6.5 km), indicating that sill intrusions occurred beneath the southern and northeastern flank of the EFJ volcano (Fig. 10a; Sigmundsson et al. 2010, Guðmundsson et al. 2010, Tarasewicz et al. 2012a). On March 20th, the EFJ 2010 eruption started effusively (Phase I) with the emission of a basaltic lava flow erupted at the Fimmvörðuháls pass (Fig. 10a); this eruptive phase lasted until April 12th. The erupted composition, BAS I (Fig. 3a), indicates a poorly evolved magma that, according to Viccaro et al. (2016), might have been involved in mixing events prior to eruption. On April 14th the eruption broke out from the summit of the volcano and became explosive (Phase IIa; Fig. 10b); its intensity decreased progressively until May 4th. During this phase, glass compositions in the SiO_2 ranges 50-52 wt% and 58-70 wt% were erupted (Fig. 3a). On May 5th the explosive activity regenerated, lasting until May 22nd (Fig. 10c). This final phase of eruptive activity (Phase IIb) was characterized by the emission of ash compositions similar to Phase IIa, but the amount of samples in the SiO_2 range 57-70 wt% was much larger in comparison to the previous phase (Fig. 3b). Tarasewicz et al. (2012a, b) suggest that the increase of activity at the beginning of May might have been triggered by new magma inputs from deeper levels (20-25 km depth; Fig. 10c).

Always consult and cite the final, published document. See http:/www.minsocam.org or GeoscienceWorld

Geophysical evidence indicates that from 1994 to 2010 seismic activity, compatible with the intrusion of different sills, occurred at depths of 5-12 km and 19-25 km (Sturkell et al. 2003; Pedersen and Sigmundsson 2004, 2006; Hjaltadóttir et al. 2009, 2015; Tarasewicz et al. 2012b). Accordingly, it appears reasonable to hypothesize that before the beginning of the eruption in March 2010, the plumbing system of EFJ consisted of a set of sills, possibly constituted by magmas with different compositions (e.g. TA and RH; Fig. 10). As indicated above, the EFJ 2010 eruption started with the output of basaltic lava flow (BAS I). During its ascent to the surface, this basalt is likely to have intersected those compositionally varied sills that were already emplaced at different depths. In particular, according to our geochemical data and modeling, BAS I may have intersected a magma batch of TA composition. Magma mixing between BAS I and TA was not completed, producing BAS II compositions that mainly occur during Phase IIa (Fig. 3). At the same time, the arrival of BAS I into the plumbing system of the volcano might have caused a general remobilization of the plumbing systems leading TA magmas to interact with more evolved magmas, such as RH. Given the similarity of the most evolved RH compositions and the rhyolitic compositions erupted during 1821 and 1823 eruptions (Fig. 2; Larsen et al. 1999), it appears reasonable to hypothesize that rhyolitic magma batches from this eruption remained at depth and were remobilized and mixed with TA compositions during the EFJ 2010 eruption. This would be in agreement with geochemical data highlighting the occurrence of glass compositions ranging from TA to RH during Phase IIa (Fig. 3). Interaction of TA and RH intensified during Phase IIb, as indicated by the occurrence of ash compositions mostly in the range TA-RH (Fig. 3).

Always consult and cite the final, published document. See http:/www.minsocam.org or GeoscienceWorld

In conclusion, by merging geophysical, petrological data and geochemical modeling, it appears that the arrival of BAS I destabilized the entire EFJ 2010 plumbing system (Fig. 10b; Tarasewicz et al. 2012b), leading to multiple mixing events between distinct magma batches that were emplaced at different times beneath the volcano. Magma mixing processes protracted with different intensities throughout the whole duration of the eruption to generate the complex and widespread compositional variability frozen in time by the eruption in the erupted ash.

Acknowledgements

This work was supported by VERTIGO Initial Training Network funded under "FP7-People-2013-ITN" (607905) and by the European Research Council with the Consolidator grant CHRONOS (612776) and PRIN n. 2010TT22SC 004 (D.P.). We acknowledge R. Astbury for proofreading of the manuscript, L. Nicconi (UNIPG, Perugia) and H. Lohringer (LMU, Munich) for the help in sample preparation, and A. Cavallo (INGV, Rome) and D. Müller (LMU, Munich) for their support in EMP analyses.

References cited

Armstrong, J.T, and Buseck P.R. (1975) Quantitative chemical analysis of individual microparticles using the electron microprobe: theoretical. Analytical Chemistry, 47, 2178-2192. Doi: 10.1021/ac6036a033

Asimov, P.D., and Ghiorso, M.S. (1998) Algorithmic modifications extending MELTS to calculate subsolidus phase relations. American Mineralogist, 83, 1127-1131. DOI: 10.2138/am-2000-0407

Always consult and cite the final, published document. See http:/www.minsocam.org or GeoscienceWorld

Baker, D.R. (1990) Chemical interdiffusion of dacite and rhyolite: anhydrous measurements at 1 atm and 10 kbar, application of transition state theory, and diffusion in zoned magma chambers. Contributions to Mineralogy and Petrology, 104, 407-423. DOI: 10.1007/BF01575619

Borisova, A., Toutain, J.P., Stefansson, A., Gouy, S., and De Parseval, P. (2012) Processes controlling the 2010 Eyjafjallajökull explosive eruption. Journal of Geophysical Research, 117, B05202. DOI: 10.1029/2012JB009213

Bryan, W.B., Finger, L.W., and Chayes, F. (1969) Estimating proportions in petrographic mixing equations by least squares approximation. Science, 163, 926-927. DOI: 10.1126/science.163.3870.926

Chayes, F. (1968) A least squares approximation for estimating the amounts of petrographic partition products. Mineralogy and Petrology Acta, 14, 111-114.

Cioni, R., Pistolesi, M., Bertagnini, A., Bonadonna, C., Hoskuldsson A., and Scateni, B. (2014) Insights into the dynamics and evolution of the 2010 Eyjafjallajökull summit eruption (Iceland) provided by volcanic ash textures. Earth and Planetary Science Letters, 394, 111–123. DOI: 10.1016/j.epsl.2014.02.051

Dahm, T., and Brandsdóttir, B. (1997) Moment tensors of microearthquakes from the Eyjafjallajökull volcano in south Iceland. Geophysical Journal International, 130, 183–192. DOI: 10.1111/j.1365-246X.1997.tb00997.x

Edwards, B.,Magnússon, E.,Thordarson, T., Guðmundsson, M.T., Höskuldsson, A., Oddsson, B., and Haklar, J. (2012) Interactions between snow/firn/ice and lava/tephra during the 2010 Fimmvörðuháls eruption, south-central Iceland. Journal of Geophysical Research, 117, B04302. DOI: 10.1029/2011JB008985

Always consult and cite the final, published document. See http:/www.minsocam.org or GeoscienceWorld

Ghiorso, M.S., and Sack, R.O. (1995) Chemical mass transfer in magmatic processes. IV. A revised and internally consistent thermodynamic model for the interpolation and extrapolation of liquid-solid equilibria in magmatic systems at elevated temperatures and pressures. Contributions to Mineralogy and Petrology, 119, 197-212. DOI: 10.1007/BF00307281

Guðmundsson, M.T., Pedersen, R., Vogfjörd, K., Thorbjarnardóttir, B., Jakobsdóttir, S., and Roberts, M. (2010) Eruptions of Eyjafjallajökull Volcano, Iceland. Eos, 91, 190–191. DOI: 10.1029/2010EO210002

Guðmundsson, M. T., Thordarson, T., Höskuldsson, Á., Larsen, G., Björnsson, H, Prata, F.J., Oddsson, B., Magnússon, E., Högnadóttir, T., Petersen, G.N., Hayward, C.L., Stevenson, J.A., and Jónsdóttir, I. (2012) Ash generation and distribution from the April-May 2010 eruption of Eyjafjallajökull, Iceland. Nature Scientific Reports, 2, 152. DOI: 10.1038/srep00572

Hibbard, M.J. (1981) The magma mixing origin of mantled feldspars. Contributions to Mineralogy and Petrology, 2, 158-170. DOI: 10.1007/BF00371956

Hjaltadóttir, S., Vogfjörð, K.S., and Slunga, R. (2009) Seismic signs of magma pathways through the crust in the Eyjafjallajökull volcano, South Iceland, Icelandic Meteorological Office Report, VI 2009, 13, 33 pp., Reykjavík, Iceland.

Hjaltadóttir, S., Vogfjörð, K.S., Hreinsdóttir, S., and Slunga, R. (2015) Reawakening of a volcano: Activity beneath Eyjafjallajökull volcano from 1991 to 2009. Journal of Volcanology and Geothermal Research, 304, 194-205. DOI: 10.1016/j.jvolgeores.2015.08.001

Always consult and cite the final, published document. See http:/www.minsocam.org or GeoscienceWorld

Hooper, A. (2008) A multi-temporal InSAR method in corporating both persistent scatterer and small baseline approaches. Geophysical Research Letters, 35, L16302. DOI: 10.1029/2008GL034654

Hooper, A., Pedersen, R., and Sigmundsson, F. (2009) The VOLUME Project — Volcanoes: Understanding Subsurface Mass Movement. Editors: Bean, C. J. et al., 13–24, University College Dublin, Ireland.

Horwell, C.J., Baxter, P.J., Hillman, S.E., Calkins, J.A., Damby, D.E., Delmelle, P., Donaldson, K., Dunster, C., Fubini, B., Kelly, F.J., Le Blond, J.S., Livi, K.J.T., Murphy, F., Nattrass, C., Sweeney, S., Tetley, T.D., Thordarson, T., and Tomatis, M. (2013) Physicochemical and toxicological profiling of ash from the 2010 and 2011 eruptions of Eyjafjallajökull and Grímsvötn volcanoes, Iceland using a rapid respiratory hazard assessment protocol. Environmental Research, 127, 63-73. DOI: 10.1016/j.envres.2013.08.011

Jarosewich, E., Nelen, J.A., and Norberg, J.A. (1980) Reference samples for electron microprobe analysis. Geostandards Newsletter, 4, 43-47. DOI: 10.1111/j.1751-908X.1980.tb00273.x

Karlsdóttir, S. (2012) The Eyjafjalljökull 2010 eruption, Iceland, Report on the 2010 Eyjafjallajökull eruption, Iceland. Editor: Barði Porkelsson, B., Report to ICAO - June 2012, International Volcanic Ash Task Force (IVATF) Fourth Meeting, Montréal, Canada.

Keiding, J.K., and Sigmarsson, O. (2012) Geothermobarometry of the 2010 Eyjafjallajökull eruption: New constraints on Icelandic magma plumbing systems. Journal of Geophysical Research, 117, B00C09. DOI: 10.1029/2011JB008829

Always consult and cite the final, published document. See http:/www.minsocam.org or GeoscienceWorld

Larsen, G., Dugmore, A.J., and Newton, A.J. (1999) Geochemistry of historical-age silicic tephras in Iceland. Holocene, 9, 463–1. DOI: 10.1191/095968399669624108

Le Bas, M.J., Lemaitre, R.W., Streckeisen, A., and Zanettin, B. (1986) A chemical classification of volcanic-rocks based on the total alkali silica diagram. Journal of Petrology, 27, 745–750. DOI: 10.1093/petrology/27.3.745

Longerich, H.P., Jackson, S.E., and Günther, D. (1996) Laser ablation inductively coupled plasma mass spectrometric transient signal data acquisition and analyse concentration calculation. Journal of Analytical Atomic Spectrometry, 11, 899-904. DOI: 10.1039/JA9961100899

Loughlin, S.C. (1995) The Eyjafjallajökull volcanic system, Southern Iceland. 319 p. Ph.D. thesis, Durham University, United Kingdom.

McDonough, W.F., and Sun, S.S. (1989) Chemical and isotopic systematics of oceanic basalts: implications for mantle composition and processes. Geological Society, Special Publications, 42, 313-345. DOI: 10.114/GSL.SP.1989.042.01.19

Miller, S.A. (2011) April 2010 UK Airspace closure: Experience and impact on the UK's air-travelling public and implications for future travel. Journal of Air Transport Management, 17, 296-301. DOI: 10.1016/j.jairtraman.2011.03008

Morgavi, D., Perugini, D., De Campos, C.P, and Dingwell, D.B. (2013a) Time evolution of chemical exchanges during mixing of rhyolitic and basaltic melts. Contributions to Mineralogy and Petrology, 166, 615-638. DOI: 10.1007/s00410-013-0894-1

Morgavi, D., Perugini, D., De Campos, C.P., Ertl-Ingrisch, W., Lavallée, Y., Morgan, L., and Dingwell, D.B. (2013b) Interactions between rhyolitic and basaltic melts unraveled by chaotic mixing experiments. Chemical Geology, 346, 199-212. DOI:

Always consult and cite the final, published document. See http:/www.minsocam.org or GeoscienceWorld

10.1016/j.chemgeo.2012.10.003

O'Regan, M. (2011) On the edge of chaos: European aviation and disrupted mobilities. Mobilities, 6, 21-30. DOI: 10.1080/17450101.2011.532649

Paton, C., Hellstrom, J., Paul, B.,Woodhead, J., and Hergt, J. (2011) Iolite: Freeware for the visualisation and processing of mass spectrometric data. Journal of Analytical Atomic Spectrometry, 26, 2508-2518. DOI: 10.1039/C1JA10172B

Pearce, N.J.G., Perkins, W.T., Westgate, J.A., Gorton, M.P., Jackson, S.E., Neal, C.R., and Chenery, S.P. (1997) A compilation of new and published major and trace element data for NIST SRM 610 and NIST SRM 612 glass reference materials. Geostandards Newsletter, 21, 115-144. DOI: 10.1111/j.1751-908X.1997.tb00538.x

Pedersen, R., and Sigmundsson, F. (2004) InSAR based sill model links spatially offset areas of deformation and seismicity for the 1994 unrest episode at Eyjafjallajökull volcano, Iceland. Geophysical Research Letters, 31, L14610. DOI: 10.1029/2004GL020368

Pedersen, R., and Sigmundsson, F. (2006) Temporal development of the 1999 intrusive episode in the Eyjafjallajökull volcano, Iceland, derived from InSAR images. Bulletin of Volcanology, 68, 377- 393. DOI: 10.1007/s00445-005-0020

Perugini, D., De Campos, C.P., Dingwell, D.B., and Dorfman, A. (2013) Relaxation of concentration variance: A new tool to measure chemical element mobility during mixing of magmas. Chemical Geology, 335, 8-23. DOI: 10.1016/j.chemgeo.2012.10.050

Perugini, D., De Campos, C.P., Dingwell, D.B., Petrelli, M., and Poli, G. (2008) Trace element mobility during magma mixing: Preliminary experimental results.

Always consult and cite the final, published document. See http:/www.minsocam.org or GeoscienceWorld

Chemical Geology, 256,146–157. DOI: 10.1016/j.chemgeo.2008.06032

Perugini, D., De Campos, C.P., Petrelli, M., and Dingwell, D.B. (2015) Concentration variance decay during magma mixing: a volcanic chronometer. Scientific Reports, 5, 14225. DOI: 10.1038/srep14225

Perugini, D., Petrelli, M., and Poli, G. (2006) Diffusive fractionation of trace elements by chaotic mixing in magmas. Earth and Planetary Science Letters, 243, 669-680. DOI: 10.1016/j.epsl.2006.01.026

Perugini, D., Ventura, G., Petrelli, M., and Poli, G. (2004) Kinematic significance of morphological structures generated by mixing of magmas: a case study from Salina Island (southern Italy). Earth and Planetary Science Letters, 222, 1051–1066. DOI: 10.1016(j.epsl.2004.03.038

Petrelli, M., Poli, G., Perugini, D., and Peccerillo, A. (2005) PetroGraph: A new software to visualize, model, and present geochemical data in igneous petrology. Geochemistry, Geophysics, Geosystems 6. Q07011. DOI: 10.1029/2005GC000932

Petrelli, M., Laeger, K., and Perugini, D. (2016a) High spatial resolution trace element determination of geological samples by laser ablation quadrupole plasma mass spectrometry: implications for glass analysis in volcanic products. Geosciences Journal, 20, 1-13. DOI: 10.1007/s12303-016-0007-z

Petrelli, M., Morgavi, D., Vetere, F.P., and Perugini, D. (2016b) Elemental imaging and petro-volcanological applications of an improved laser ablation inductively coupled quadrupole plasma mass spectrometry, Periodico di Mineralogia, 85, 25-39. DOI: 10.2451/2015PM0465

Reid, F. (1983) Origin of rhyolitic rocks of the Taupo Volcanic Zone, New Zealand.

Always consult and cite the final, published document. See http:/www.minsocam.org or GeoscienceWorld

Journal of Volcanology and Geothermal Research, 15, 315-338. DOI: 10.1016/0377-0273(83)90105-1

Sigmarsson, O., Vlastelic, I., Andreasen, R., Bindeman, I., Devidal, J.-L., Moune, S., Keiding, J.K., Larsen, G., Höskuldsson, A., and Thordarson, T. (2011) Remobilization of silicic intrusion by mafic magmas during the 2010 Eyjafjallajökull eruption. Solid Earth, 2, 271-281. DOI: 10.5194/se-2-271-2011

Sigmarsson, O., Condomines, M., and Gauthier, P.-J. (2015) Excess ^{210}Po in 2010 Eyjafjallajökull tephra (Iceland): Evidence for pre-eruptive gas accumulation. Earth and Planetary Science Letters, 427, 66-73. DOI: 10.1016/j.epsl.2015.06054

Sigmundsson, F., Hreinsdóttir, S., Hooper, A., Árnadóttir, T., Pedersen, R., Roberts, M. J., Óskarsson, N., Auriac, A., Decriem, J., Einarsson, P., Geirsson, H., Hensch, M., Ófeigsson, B. G., Sturkell, E., Sveinbjörnsson, H., and Feigl, K.L. (2010) Intrusion triggering of the 2010 Eyjafjallajökull eruption. Nature, 468, 426-430. DOI: 10.10138/nature09558

Sigmundsson, F., Hreinsdóttir, S., Ofeigsson, B.G., Hooper, A.J., and Geirsson, H. (2012) Eruptive cycles at Icelandic volcanoes: Constraints on inflation/deflation patterns from geodetic measurements and modeling. AGU Fall Meeting Abstracts 1, 02.

Slaby, E. (2011) Chaotic three-dimensional distribution of Ba, Rb, and Sr in feldspar megacrysts grown in an open magmatic system. Contributions to Mineralogy and Petrology, 161, 909-927. DOI: 10.1007(s00410-011-0631-6

Always consult and cite the final, published document. See http:/www.minsocam.org or GeoscienceWorld

Störmer, J.C., and Nicholls, J. (1978) XLFRAC: a program for the interactive testing of magmatic differentiation models. Computers & Geosciences, 4, 143-159. DOI: 10.1016/0098-3004(78(90083-3

Sturkell, E., Einarsson, P., Sigmundsson, F., Geirsson, H., Olafsson, H., Pedersen, R., de Zeeuwvan Dalfsen, E., Linde, A.T., Sacks,S.I., and Stefansson, R. (2006) Volcano, geodesy and magma dynamics in Iceland. Journal of Volcanology and Geothermal Research, 150, 14–34. DOI: 10.1016/j.jvolgeores.2005.07.010

Sturkell, E., Einarsson, P., Sigmundsson, F., Hooper, A., Ofeigsson, B.G., Geirsson, H., and Ialsson, H.O. (2010) 2 Katla and Eyjafjallajökull Volcanoes. Developments in Quaternary Science, 13, 5–21. DOI: 10.1016/S1571-0866(09)01302-5

Sturkell, E., Sigmundsson, F., and Einarsson, P. (2003) Recent unrest and magma movements at Eyjafjallajökull and Katla volcanoes, Iceland. Journal of Geophysical Research, 108, 2369. DOI: 10.1029/2001JB000917

Tarasewicz, J., Brandsdóttir, B., White, R.S., Hensch, M., and Thorbjarnardóttir, B. (2012a) Using microearthquakes to track repeated magma intrusions beneath the Eyjafjallajökull stratovolcano, Iceland. Journal of Geophysical Research, 117, B00C06. DOI: 10.1029/2011JB008751

Tarasewicz, J., White, R.S., Woods, A.W., Brandsdóttir, B., and Guðmundsson, M.T. (2012b) Magma mobilization by downward-propagating de- compression of the Eyjafjallajökull volcanic plumbing system. Geophysical Research Letters, 39, L19309. DOI: 10.1029/2012GL053518

Viccaro, M., Giuffrida, M., Nicotra, E., and Cristofolini, R. (2016) Timescales of magma and migration recorded by olivine crystals in basalts of the March-April 2010

Always consult and cite the final, published document. See http:/www.minsocam.org or GeoscienceWorld

erutpion at Eyjafjallajökull volcano, Iceland. American Mineralogist, 101, 222-230. DOI: 10.2138/am-2016-5365

Watson, E.B. (1976) Two-liquid partition coefficients: Experimental data and geochemical implications. Contributions to Mineraogy and Petrolog, 56, 119-134. DOI: 10.1007/BF00375424

Watson, E.B., and Jurewicz, S.R. (1984) Behavior of alkalies during diffusive interaction of granitic xenoliths with basaltic magma. Journal of Geology, 92, 121-131. DOI: jstor.org/stable/30062260

Wilson, S.A. (1997) The collection, preparation, and testing of USGS reference material BCR-2, 557 Columbia River, Basalt. Open-File Rep. 98 p., United States Geological Survey, United States.

Zhang, Y. (2008) Geochemical Kinetics. 664 pp, Princeton University Press. ISBN: 9780691124322

List of figure captions

Figure 1. Relief map (after Sigmarsson et al. 2011) with main ice-caps, roads and towns showing the location of Eyjafjallajökull, Katla, Vestmannaeyar and Surtsey volcanoes. The location of samples collected from the explosive phase of EFJ 2010 eruption deposited between April 15th to May 22nd are also shown as black stars. Numbers indicate sample number as reported in Table i in the Supplementary Material. The black arrow between Eyjafjallajökull and Katla volcanoes indicate the Fimmvörðuháls pass, i.e. the location of the effusive flank eruption during Phase I. WVZ, NVZ and EVZ in the inset on top-left of the figure indicate western, northern and eastern volcanic zone, respectively.

Always consult and cite the final, published document. See http:/www.minsocam.org or GeoscienceWorld

Figure 2. BSE images showing some representative petrographic characteristics of lava clasts and ash fragments from the summit eruption. (a) Ash particles with different groundmass compositions (indicated by arrows and SiO_2 contents) within the same sample. (b) Trachyandesitic enclave (light grey color) in a trachydacitic matrix with elongated plagioclase microlites. (c) Homogeneous olivine (top-right corner) and normal zoned plagioclase phenocrysts. (d) Resorbed plagioclase with inclusion of Fe-rich clinopyroxene. (e) Normal zoned olivine phenocrysts with chromium spinel inclusions in a fully crystalline matrix. (f) Reverse zoned clinopyroxene with a rounded and resorbed core.

Figure 3. Total alkali vs. silica (TAS) diagrams **(**Le Bas et al. 1986) for lava and tephra of the EFJ 2010 eruption. (a) Compositions of Phase I (GL Phase I - black squares: composition of groundmass glass of BAS I; WR Phase I - grey diamonds: whole rock composition of BAS I) (Sigmundsson et al. 2010; Sigmarsson et al. 2011; Keiding and Sigmarsson 2012; Borisova et al. 2012). Glass compositions of Phase IIa measured in this study (GL Phase IIa this study) in light grey squares (14.04.-04.05.2010). Glasses of Phase IIa (GL Phase IIa) from Sigmarsson et al. (2011), Keiding and Sigmarsson (2012), Borisova et al. (2012) and Cioni et al. (2014) are also reported in filled grey squares. Glass compositions of the EFJ 1821-23 eruption (GL RH1821 - black crosses) after Larsen et al. (1999) and Sigmarsson et al. (2011) are also shown. **(b)** Glass compositions of Phase IIb (erupted between 06.-22.05.2010) measured in this study (GL Phase IIb this study). Error bars (representing standard deviations from the mean) are also reported.

Always consult and cite the final, published document. See http:/www.minsocam.org or GeoscienceWorld

Figure 4. Selected major element vs. silica diagrams of erupted products of the EFJ eruptions. Symbols as in Figure 3. Error bars (representing standard deviations from the mean) are also reported.

Figure 5. Selected trace element vs. silica diagrams of erupted products in lava and tephra of the EFJ 2010 eruption. Symbols as in Figure 3. Error bars (representing standard deviations from the mean) are also reported.

Figure 6. Ocean Island Basalt (McDonough and Sun 1989) normalized diagram of glasses measured by LA-ICP-MS in the present study and literature data. Black squares represent GL BAS I from Phase I (Borisova et al. 2012); grey and light grey areas represent GL BAS II and trachyandesite to rhyolite compositions (GL TA-RH), respectively, measured in this study from Phase II.

Figure 7. Representative plots showing the modeled liquid lines of descent (LLDs) for MgO and CaO versus SiO_2 at 0.5 wt% H_2O in the temperature range 900-1340 °C for rocks and glasses of the Eyjafjallajökull 2010 eruption calculated by MELTS (Ghiorso and Sack 1995; Asimov and Ghiorso 1998) for different starting parental melt compositions (a) and (b) WR BAS I; (c) and (d) GL BAS II; (e) and (f) GL BAS II, and (g) and (h) GL TA. LLDs are shown for different pressure and oxygen buffer. Note that LLDs of none of the models is able to explain the compositional variability based upon

Always consult and cite the final, published document. See http:/www.minsocam.org or GeoscienceWorld

fractional crystallization (see text for details). The complete set of models at different conditions is reported in the Supplementary Material 'xi'.

Figure 8. Representative binary inter-elemental plots of trace elements for glass compositions between 57 to 69 wt% SiO_2 (TA to RH of Phase IIb), illustrating the extreme variability of correlation between couples of elements. The patterns range from ca. linear to completely scattered.

Figure 9. Concentration frequency histograms of representative major and trace elements of groundmass glasses of the EFJ 2010 eruption (Phase IIb). The most mobile elements during mixing display a bell-shaped Gaussian distribution, indicating the production of a large amount of hybrid compositions. Gaussian fitting for most mobile elements such as Na_2O (g), Cs (d), Pr (f) and Gd (h) allow for estimating the hybrid concentration of the element (C_H) to be used in the estimate of initial proportions of end-member magmas (eq. 1 in the text).

Figure 10. Cartoon modified after Tarasewicz et al. (2012b) illustrating the possible evolution of the EFJ 2010 eruption in time. Sills with different compositions, possibly emplaced at different depth and at different times prior to EFJ 2010 eruption are also reported in different colors. (a) Phase I: fissure eruption (BAS I) at Fimmvörðuháls pass after formation of a basaltic sill and dyke since the end of 2009; arrival of new basaltic magma reactivates the plumbing system, constituted by magma batches that were already emplaced as sills. (b) Phase IIa: explosive summit eruption generates ash samples (e.g.

Always consult and cite the final, published document. See http:/www.minsocam.org or GeoscienceWorld

Sigmarsson et al. 2011) containing mainly trachyandesite (TA) glass, a more evolved basalt (BAS II) and rhyolitic melts (RH). (c) Phase IIb: explosive summit generating ash samples with continuous compositions between TA and RH glasses and minor BAS II.

Always consult and cite the final, published document. See http:/www.minsocam.org or GeoscienceWorld

This is a preprint, the final version is subject to change, of the American Mineralogist (MSA)
Cite as Authors (Year) Title. American Mineralogist, in press.
(DOI will not work until issue is live.) DOI: http://dx.doi.org/10.2138/am-2017-5860

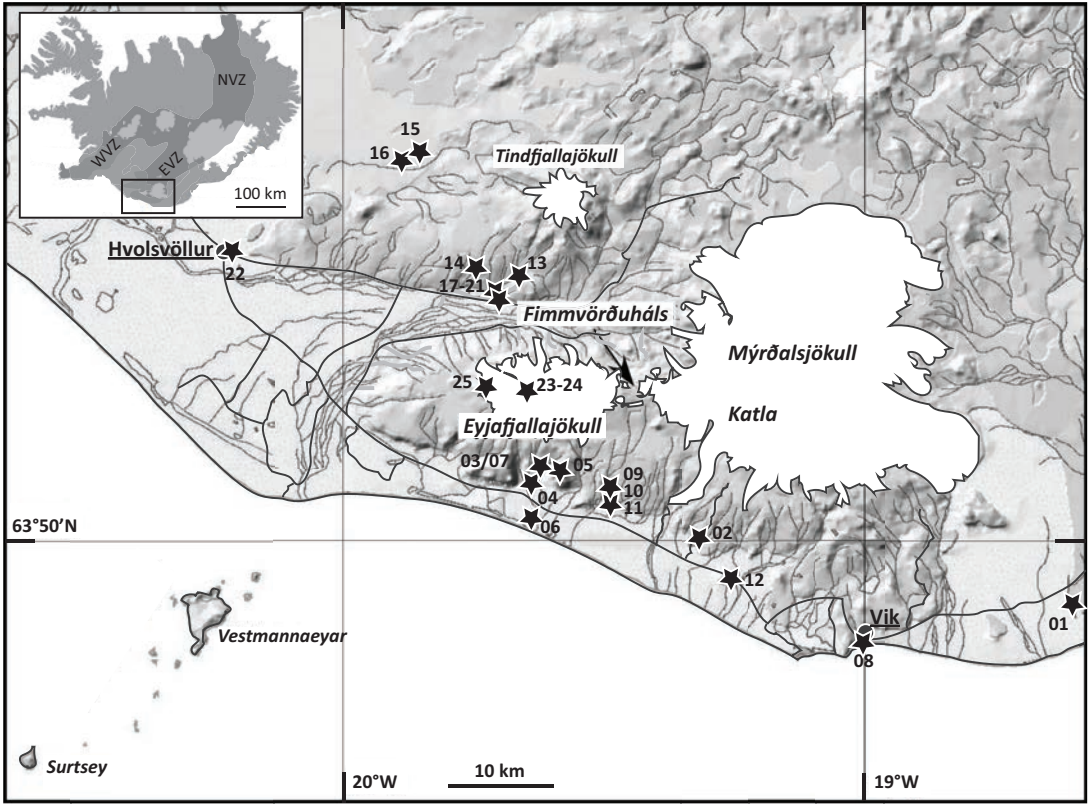

Always consult and cite the final, published document. See http:/www.minsocam.org or GeoscienceWorld

This is a preprint, the final version is subject to change, of the American Mineralogist (MSA)
Cite as Authors (Year) Title. American Mineralogist, in press.
(DOI will not work until issue is live.) DOI: http://dx.doi.org/10.2138/am-2017-5860

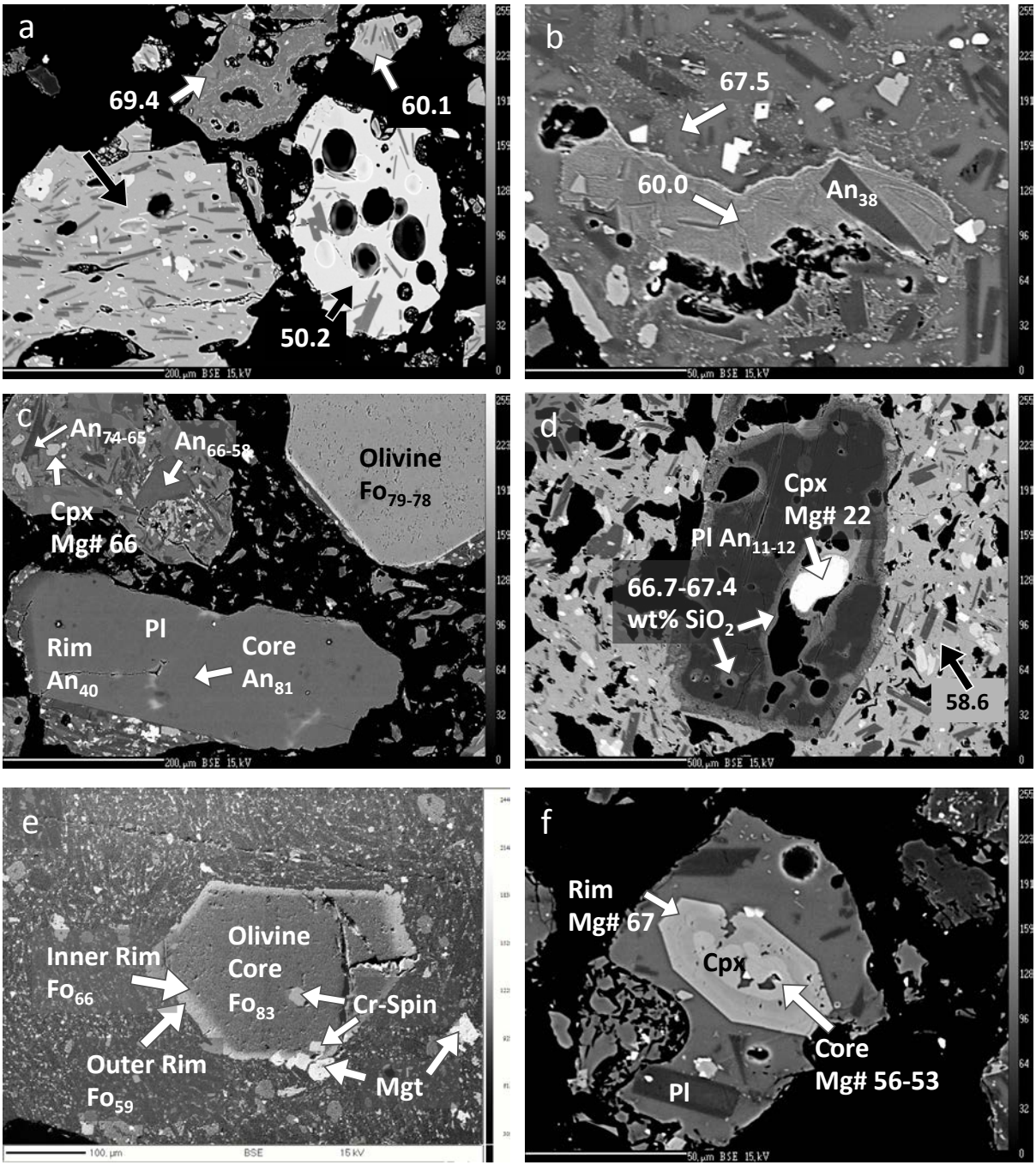

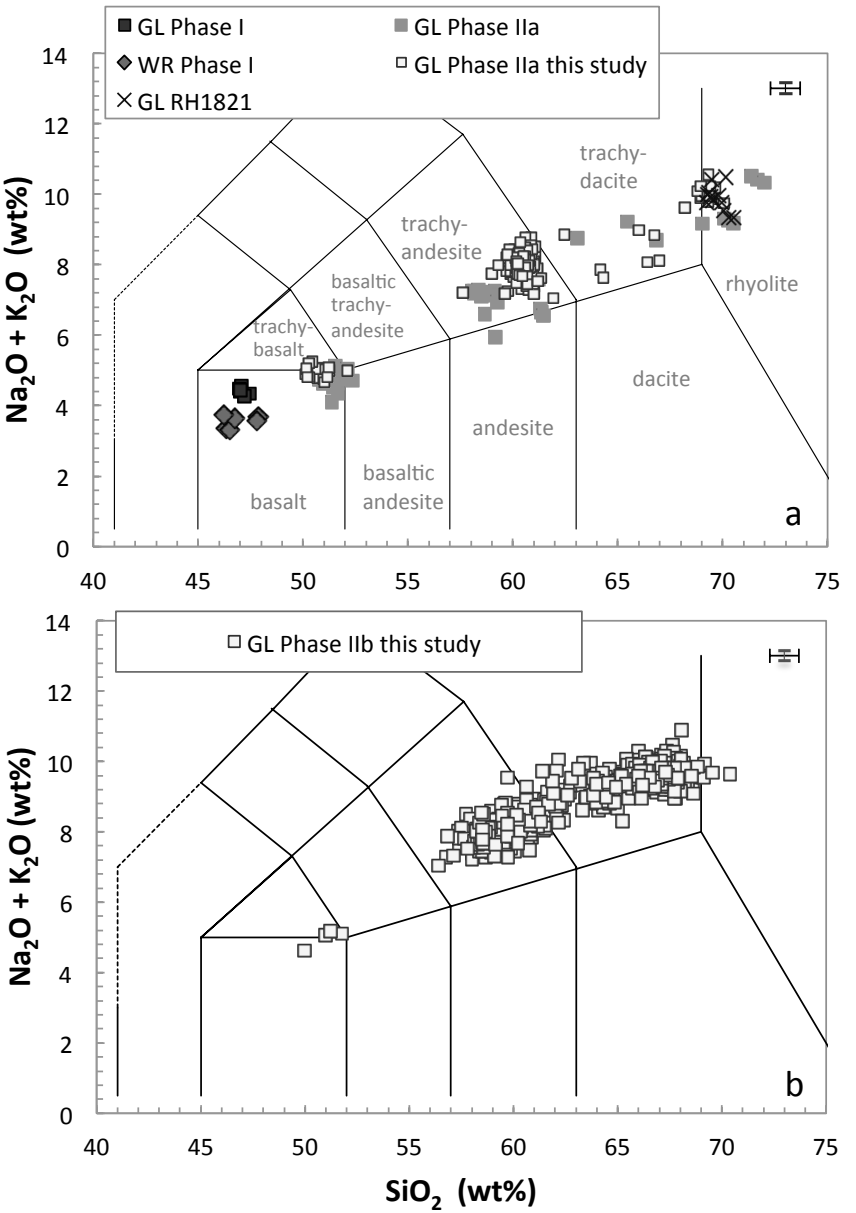
GL Phase I
GL Phase IIa
WR Phase I
GL Phase IIa this study
GL RH1821
trachy-dacite
trachy-andesite
basaltic trachy-andesite
trachy-basalt
rhyolite
dacite
andesite
basaltic andesite
basalt
a
GL Phase IIb this study
b
$Na_2O + K_2O$ (wt%)
SiO_2 (wt%)
0
2
4
6
8
10
12
14
40
45
50
55
60
65
70
75

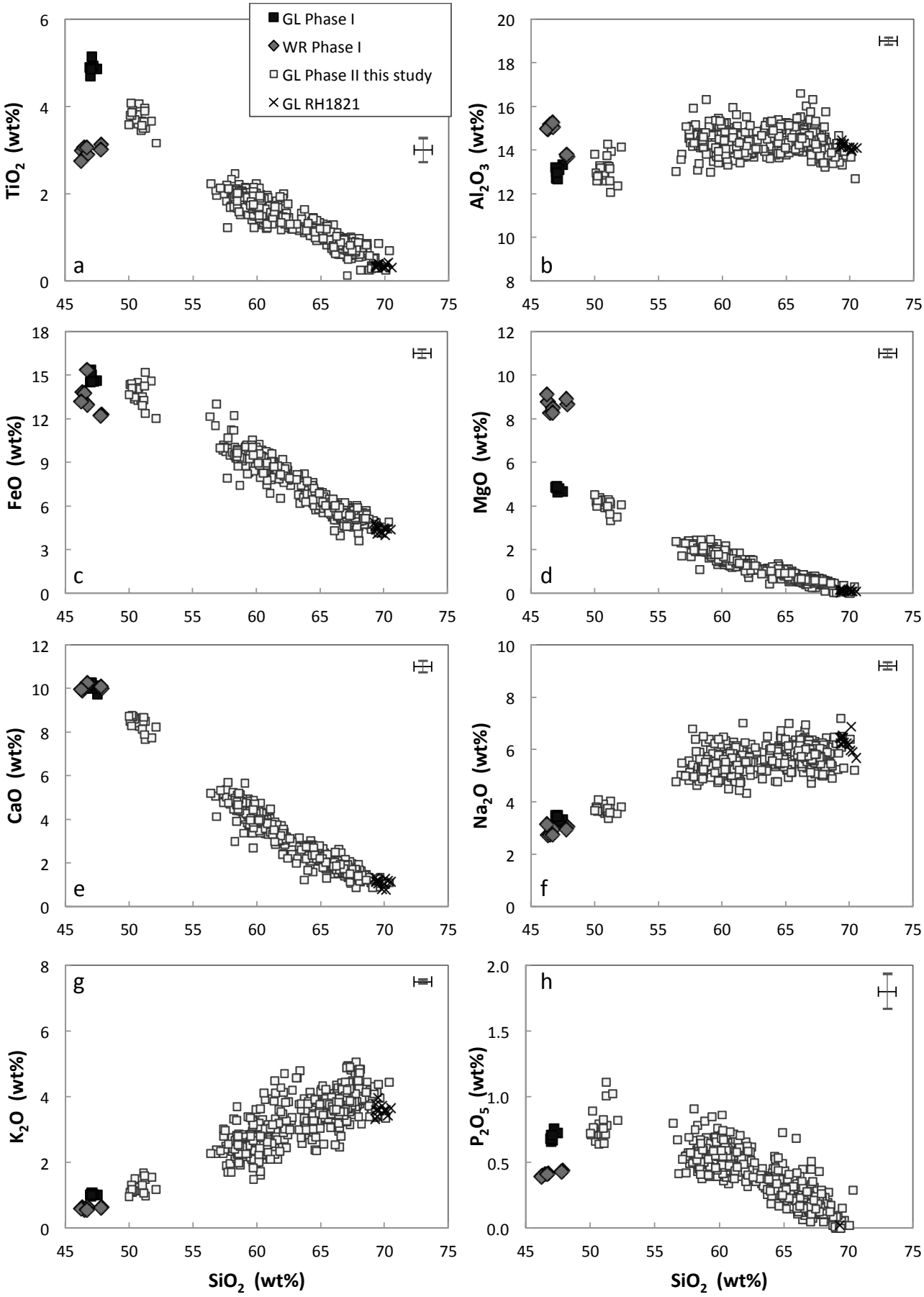
GL Phase I
WR Phase I
GL Phase II this study
GL RH1821
a
b
c
d
e
f
g
h
TiO2 (wt%)
Al2O3 (wt%)
FeO (wt%)
MgO (wt%)
CaO (wt%)
Na2O (wt%)
K2O (wt%)
P2O5 (wt%)
SiO2 (wt%)
SiO2 (wt%)

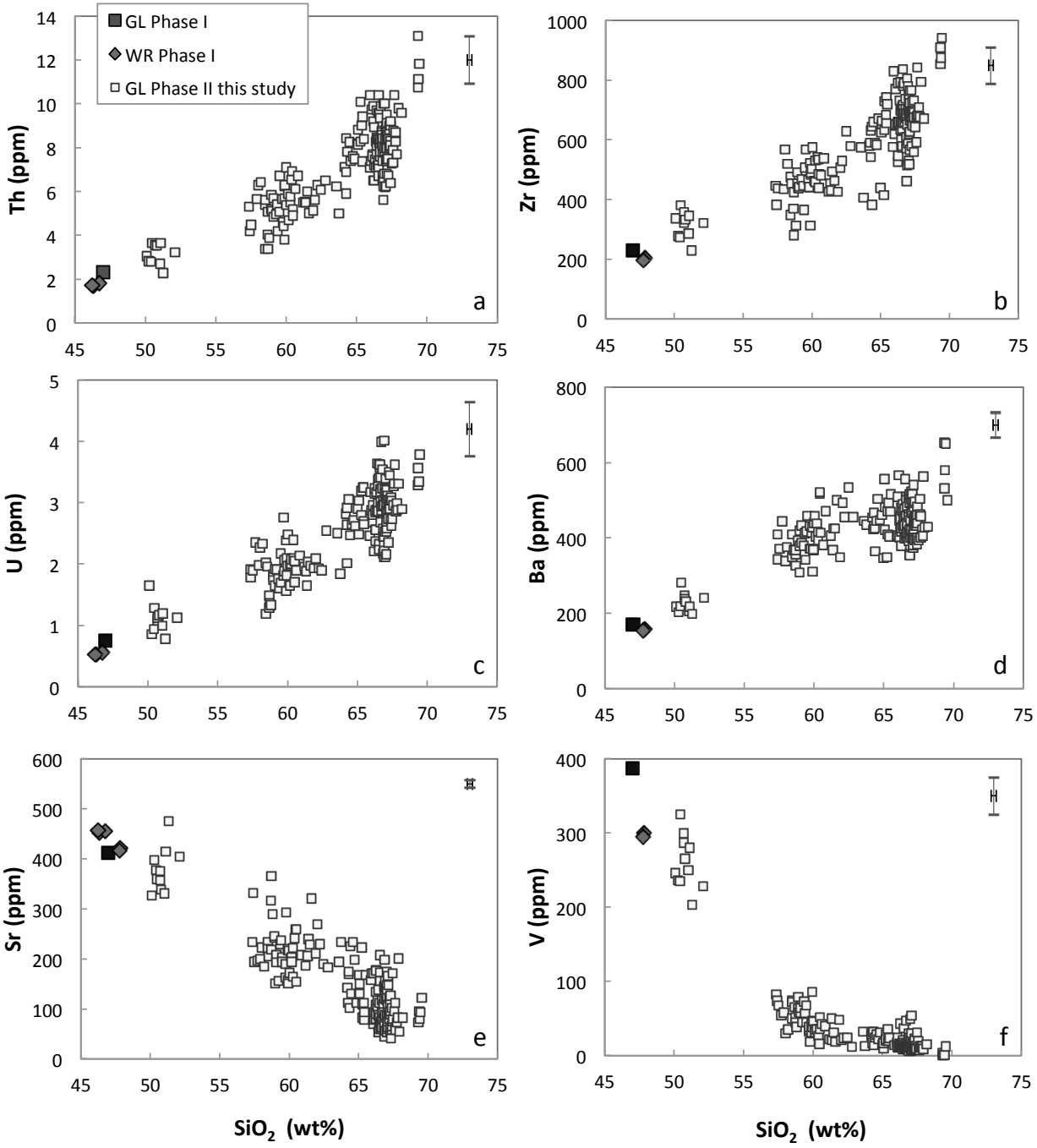
GL Phase I
WR Phase I
GL Phase II this study
Th (ppm)
Zr (ppm)
U (ppm)
Ba (ppm)
Sr (ppm)
V (ppm)
a
b
c
d
e
f
SiO2 (wt%)
SiO2 (wt%)

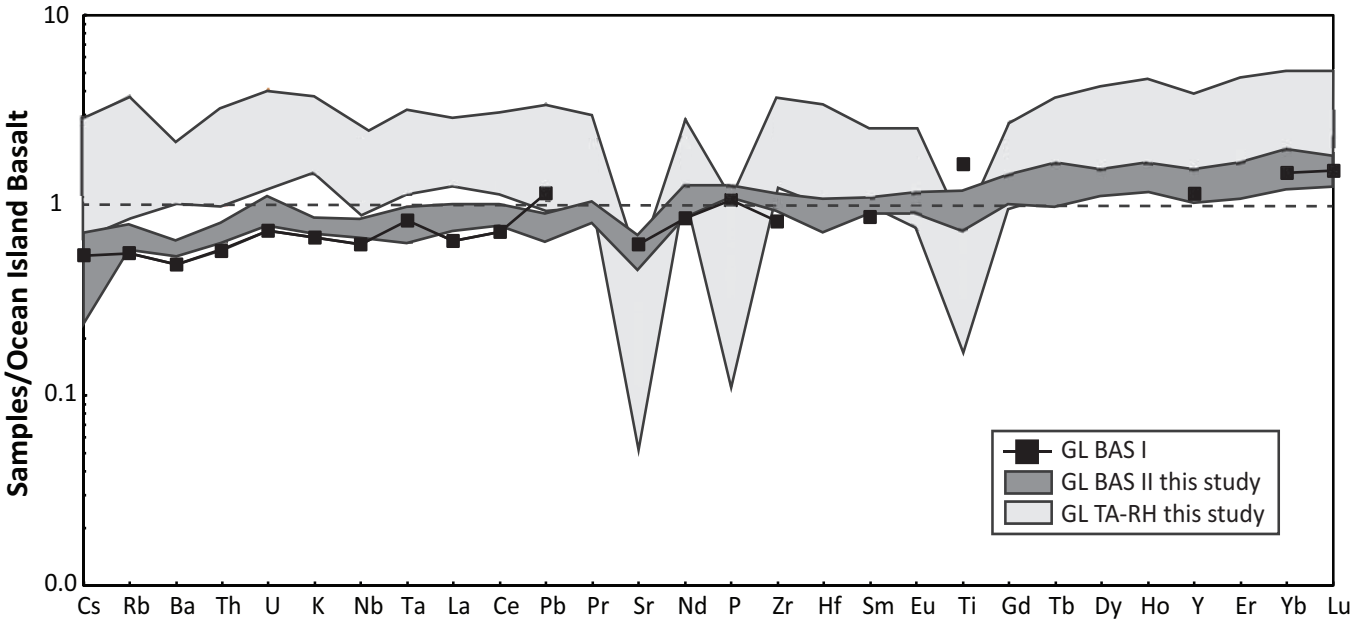
Samples/Ocean Island Basalt
10
1
0.1
0.0
Cs Rb Ba Th U K Nb Ta La Ce Pb Pr Sr Nd P Zr Hf Sm Eu Ti Gd Tb Dy Ho Y Er Yb Lu
GL BAS I
GL BAS II this study
GL TA-RH this study

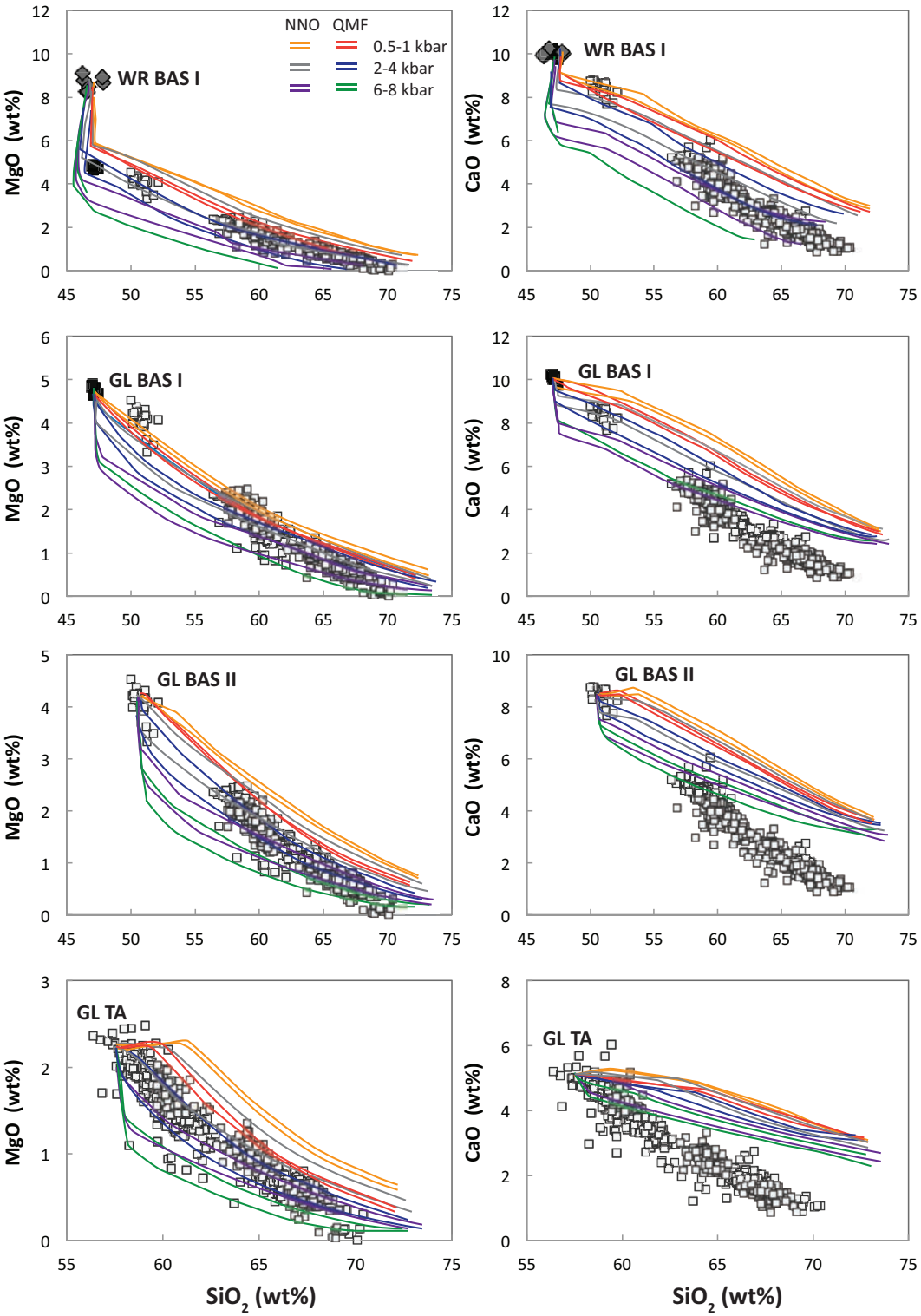
NNO
QMF
0.5-1 kbar
2-4 kbar
6-8 kbar
WR BAS I
GL BAS I
GL BAS II
GL TA
MgO (wt%)
CaO (wt%)
SiO2 (wt%)

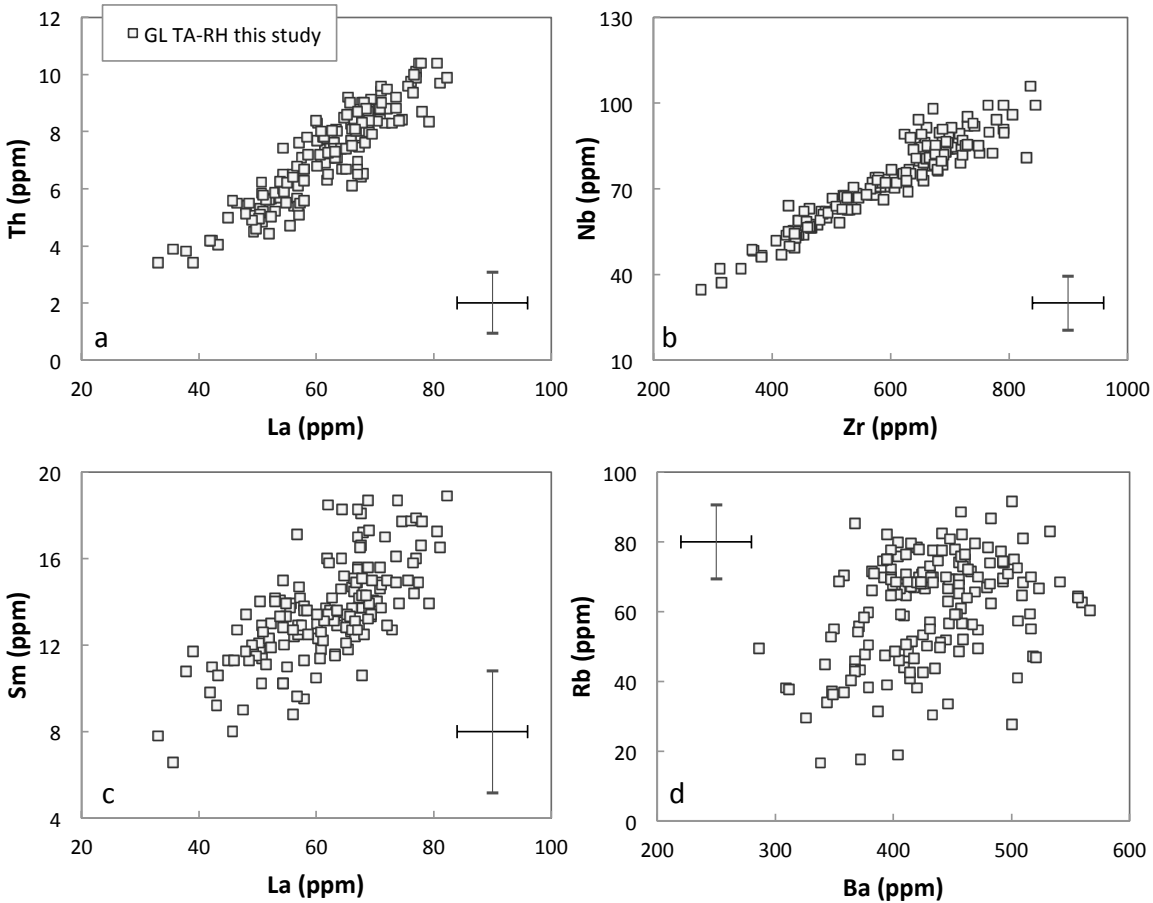
GL TA-RH this study
Th (ppm)
La (ppm)
a
Nb (ppm)
Zr (ppm)
b
Sm (ppm)
La (ppm)
c
Rb (ppm)
Ba (ppm)
d

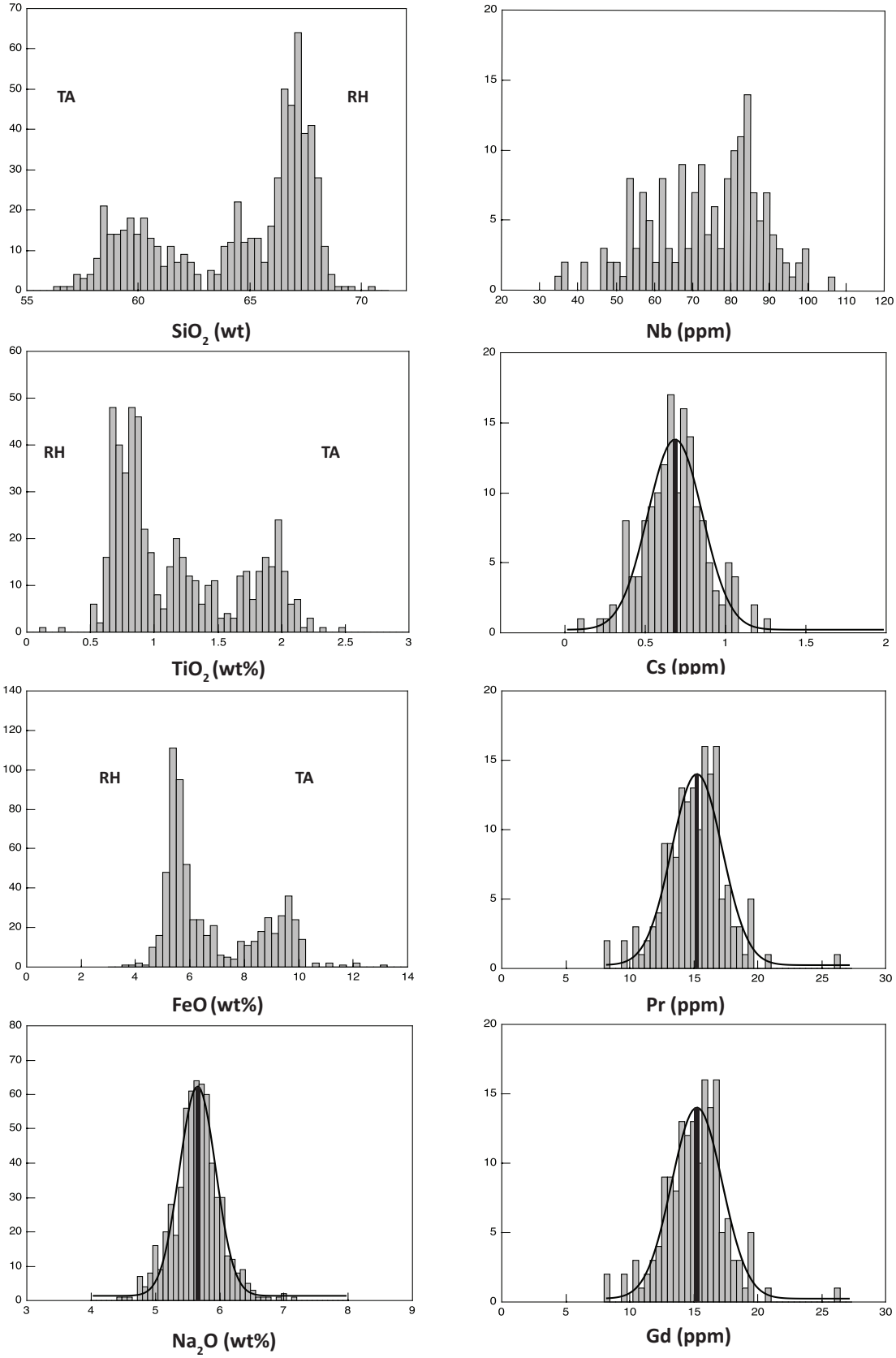
TA
RH
SiO2 (wt)
Nb (ppm)
RH
TA
TiO2 (wt%)
Cs (ppm)
RH
TA
FeO (wt%)
Pr (ppm)
Na2O (wt%)
Gd (ppm)

This is a preprint, the final version is subject to change, of the American Mineralogist (MSA)
Cite as Authors (Year) Title. American Mineralogist, in press.
(DOI will not work until issue is live.) DOI: http://dx.doi.org/10.2138/am-2017-5860

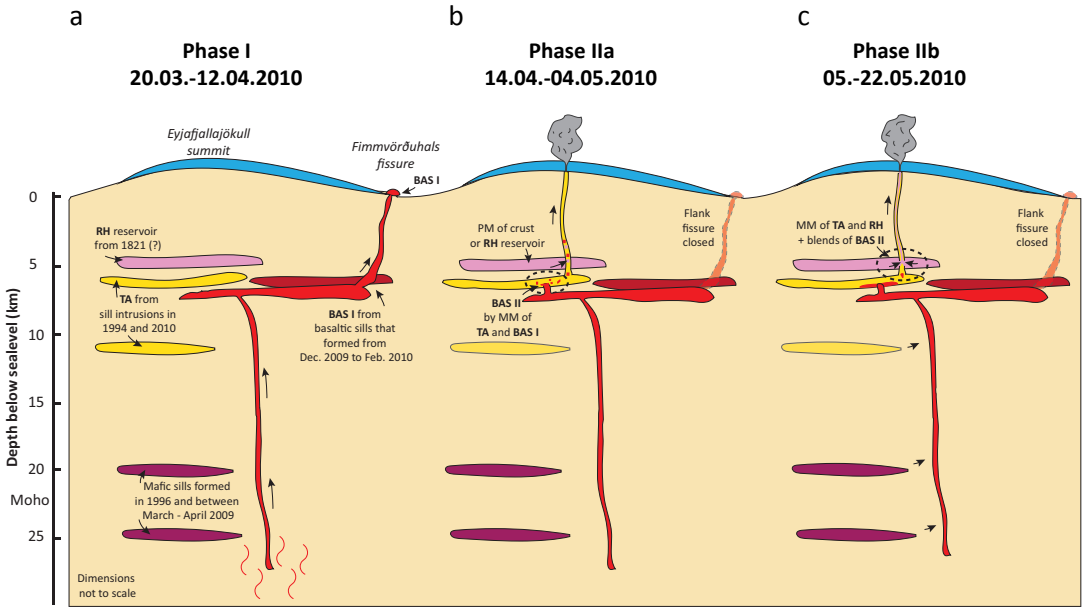

Always consult and cite the final, published document. See http:/www.minsocam.org or GeoscienceWorld

Table 1: Results of magma mixing calculations using the least-squares mass balance model after Störmer and Nicholls (1978). Abbreviations: GL - glass, BAS - basalt, TA - trachyandesite, RH - rhyolite.

Hybrid Component	**Felsic Component**	**Mafic Component**	$\sum^{a}$	**Fraction of mafic melt**	**Fraction of felsic melt**
GL BAS II[b]	GL TA[b]	GL BAS I[c]	0.75	0.67	0.33
GL TA[b]	GL RH[b]	GL BAS II[b]	3.49	0.61	0.39
GL TA 59[b, d]	GL RH[b]	GL TA[b]	0.06	0.85	0.15
GL TA 61[b, d]	GL RH[b]	GL TA[b]	0.13	0.72	0.28
GL TA 63[b, d]	GL RH[b]	GL TA[b]	0.22	0.51	0.49
GL TA 65[b, d]	GL RH[b]	GL TA[b]	0.47	0.34	0.66
GL TA 67[b, d]	GL RH[b]	GL TA[b]	0.37	0.16	0.84

[a] calculated after Störmer and Nicholls (1978).

[b] this study.

[c] Sigmarsson et al. (2011), Keiding and Sigmarsson et al. (2012), Borisova et al. (2012).

[d] number indicates SiO_2 in wt%.

Table 2: Calculated felsic melt proportions (X) for Phase IIb. Abbreviations: C_F, C_M and C_H - concentrations of felsic, mafic and hybrid components, respectively. In Phase IIb C_H = maximum of Gaussian Curve.

	C_F	C_M	C_H	C_F-C_M	C_H-C_M	X [a]
Na_2O	7.14	4.5	5.67	2.64	1.17	0.44
Ga	47.0	17.6	27.05	29.40	9.45	0.32
Rb	117.7	16.6	69.87	101.10	53.27	0.53
Y	119.0	23.1	61.67	95.90	38.57	0.40
Cs	1.5	0.3	0.71	1.25	0.45	0.36
La	93.0	26.0	61.89	67.00	35.89	0.54
Ce	226.0	60.0	128.90	166.00	68.90	0.42
Pr	26.2	6.5	15.30	19.70	8.80	0.45
Nd	111.0	29.9	62.43	81.10	32.53	0.40
Sm	21.7	7.1	13.33	14.60	6.23	0.43
Gd	26.3	4.8	12.49	21.50	7.69	0.36
Tb	3.8	0.6	1.91	3.22	1.33	0.41
Dy	25.1	4.0	11.53	21.10	7.53	0.36
Ho	4.5	0.9	2.33	3.61	1.41	0.39
Er	12.9	1.6	6.21	11.32	4.63	0.41
Tm	1.6	0.2	0.91	1.41	0.75	0.53
Lu	1.75	0.35	0.85	1.40	0.50	0.36
Pb	11.90	2.90	6.07	9.00	3.17	0.35

[a] $X = (C_H - C_M)/(C_F - C_M)$